surface density Σ follows a power law $\Sigma(r) = \Sigma_o (r_{AU}/370)^q$, with an index q equal to $-3/2$, as the one inferred for the solar nebula or for extrasolar nebulae (*20*, *21*), we derived a disk dust mass of 40 Earth masses within 370 AU. This lower limit is compatible with the mass of 500 Earth masses derived from the observed 1.3-mm flux (*22*). The dust mass derived here is three to four orders of magnitude larger than the dust mass observed in debris disks and Kuiper belt–like structures found around more-evolved A stars such as β-Pictoris, Vega, Fomalhaut, and HR 4796 (*4*). The dust around these Vega-like stars is thought to be produced by collisions of larger bodies, whose total mass in the case of β-Pictoris has been estimated to be on the order of 100 Earth masses (*23*). Therefore, the dust mass observed around HD 97048 is similar to the mass invoked for the (undetected) parent bodies in more-evolved systems. HD 97048's disk is thus most likely a precursor of debris disks observed around more-evolved A stars. This finding is coherent with the HD 97048 age of ~3 million years, estimated from evolutionary tracks. Another argument in favor of the early evolutionary stage of the system is the presence of a large amount of gas required to support the flaring structure revealed by our observations. Part of the gas has been recently detected, thanks to observations of the molecular hydrogen emission at 2.12 μm (*24*). Assuming that the canonical interstellar gas-to-dust mass ratio of 100 holds, we estimate a total minimum disk mass of 0.01 solar masses, like the estimated minimum mass for the proto-planetary disk around the Sun (*20*).

Because the disk surrounding HD 97048 has a mass surface density comparable to that of the minimum proto-planetary nebula around the Sun, it is worth studying the prospects for planet formation in this environment. Planet formation models are divided into two categories: gravitational instabilities (*25*) and core accretion (*26*). It seems improbable that giant planets will form by means of gravitational instabilities, because the Toomre stability criterion coefficient, equal to $H_g/r\ M_\odot/(r^2\Sigma)$, is >> 1 (*27*). Considering the alternative core accretion scenario by which planets coagulate from initially μm-sized dust (*28*, *29*), it also appears improbable that cores of giant planets are present in the outer regions because of the very long local orbital time scales. Although regions within 40 AU have not been resolved by our observations, it is tempting to extrapolate the surface density from the outer regions and investigate the predictions of planet formation models for the inner regions; inside 10 AU, planetary embryos may be present. Follow-up observations at higher angular resolution with the mid-IR instrument of the ESO Very Large Telescope interferometer will allow probing these regions.

References and Notes

1. The Extrasolar Planet Encyclopaedia presents a comprehensive list of all known exoplanets (www.obspm.fr/planets).
2. C. R. O'Dell, S. V. W. Beckwith, *Science* **276**, 1355 (1997).
3. A comprehensive list of spatially resolved disks is available (www.circumstellardisks.org).
4. J. S. Greaves, *Science* **307**, 68 (2005).
5. T. Takeuchi, C. J. Clarke, D. N. C. Lin, *Astrophys. J.* **627-1**, 286 (2005).
6. J. Setiawan *et al.*, *Astron. Astrophys.* **437**, L31 (2005).
7. B. A. Smith, R. J. Terrile, *Science* **226**, 1421 (1984).
8. G. Meeus *et al.*, *Astron. Astrophys.* **365**, 476 (2001).
9. E. I. Chiang *et al.*, *Astrophys. J.* **547**, 1077 (2001).
10. V. Mannings, A. I. Sargent, *Astrophys. J.* **529**, 391 (2000).
11. C. Grady *et al.*, *Astrophys. J.* **630**, 958 (2005).
12. B. Acke, M. E. van den Ancker, *Astron. Astrophys.* **426**, 151 (2004).
13. J. L. Puget, A. Leger, *Annu. Rev. Astron. Astrophys.* **27**, 161 (1989).
14. P.-O. Lagage *et al.*, *The Messenger* **117**, 12 (2004).
15. M. E. van den Ancker, D. de Winter, H. R. E. Tjin A Djie, *Astron. Astrophys.* **330**, 145 (1998).
16. C. Van Kerckhoven, A. G. G. Tielens, C. Waelkens, *Astron. Astrophys.* **384**, 568 (2002).
17. T. Prusti, A. Natta, F. Palla, *Astron. Astrophys.* **292**, 593 (1994).
18. R. van Boekel *et al.*, *Astron. Astrophys.* **418**, 177 (2004).
19. V. Ossenkopf, Th. Henning, *Astron. Astrophys.* **291**, 943 (1994).
20. S. J. Weidenschilling, *Astrophys. Space Sci.* **51**, 153 (1977).
21. M. J. Kuchner, *Astrophys. J.* **612**, 1147 (2004).
22. Th. Henning, A. Burkert, R. Launhardt, Ch. Leinert, B. Stecklum, *Astron. Astrophys.* **336**, 565 (1998).
23. P. Artymowicz, *Annu. Rev. Earth Planet. Sci.* **25**, 175 (1997).
24. J. S. Weintraub, J. S. Bary, J. H. Kastner, S. J. Shukla, K. Chynoweth, in *Proceedings of the Protostars and Planets V Conference*, Waikoloa, HI, 24 to 28 October, 2005, B. Reipurt, D. Jewitt, K. Keil, Eds. (LPI Contribution Number 1286, Univ. Arizona Press, Tucson, 2006), p. 8197.
25. R. H. Durisen *et al.*, in *Protostars and Planets V*, B. Reipurt, D. Jewitt, K. Keil, Eds. (Univ. of Arizona Press, Tucson, 2006), in press; preprint (www.ifa.hawaii.edu/UHNAI/ppv.htm).
26. J. J. Lissauer, *Annu. Rev. Astron. Astrophys.* **31**, 129 (1993).
27. A. Toomre, *Astrophys. J.* **139**, 1217 (1964).
28. S. Ida, D. N. C. Lin, *Astrophys. J.* **604-1**, 388 (2004).
29. P. Goldreich, Y. Lithwick, R. Sari, *Astrophys. J.* **614-1**, 497 (2004).

30. This work was based on observations carried out at the ESO, Paranal, Chile. The VISIR could not have been built without contributions from many people, including G. Durand, Y. Rio, M. Authier, C. Lyraud, and J. Pragt. We also thank A. Palacio, P. Nghiem, and C. Martin for discussions about the age of HD 97048, as well as F. Masset for discussions about gravitational instabilities.

Supporting Online Material

www.sciencemag.org/cgi/content/full/1131436/DC1
Figs. S1 and S2

19 June 2006; accepted 12 September 2006
Published online 28 September 2006;
10.1126/science.1131436
Include this information when citing this paper

The Phase-Dependent Infrared Brightness of the Extrasolar Planet υ Andromedae b

Joseph Harrington,[1,2] Brad M. Hansen,[3]* Statia H. Luszcz,[2,4] Sara Seager,[5] Drake Deming,[6] Kristen Menou,[7] James Y.-K. Cho,[8] L. Jeremy Richardson[9]

The star υ Andromedae is orbited by three known planets, the innermost of which has an orbital period of 4.617 days and a mass at least 0.69 that of Jupiter. This planet is close enough to its host star that the radiation it absorbs overwhelms its internal heat losses. Here, we present the 24-micrometer light curve of this system, obtained with the Spitzer Space Telescope. It shows a variation in phase with the orbital motion of the innermost planet, demonstrating that such planets possess distinct hot substellar (day) and cold antistellar (night) faces.

Last year, two independent groups (*1*, *2*) reported the first measurements of the infrared light emitted by extrasolar planets orbiting close to their parent stars. These "hot Jupiter" (*3*) planets have small enough orbits that the energy they absorb from their hosts dominates their own internal energy losses. How they absorb and reradiate this energy is fundamental to understanding the behavior of their atmospheres. One way to address this question is to monitor the emitted flux over the course of an orbit to see whether the heat is distributed asymmetrically about the surface of the planet.

We have observed the υ Andromedae system with the 24-μm channel of the Multiband Imaging Photometer for Spitzer (MIPS) (*4*) aboard the Spitzer Space Telescope (*5*). We took 168 3-s images at each of five epochs spread over 4.46 days (97% of the 4.617-day orbital period of υ Andromedae b) beginning on 18 February 2006 at 12:52 UTC. After rejecting frames with bad pixels near the star and those with Spitzer's "first frame effect" (*1*) (2% to 8% of the data, depending on epoch), we measured the flux of the system and that of the surrounding sky by using both subpixel, interpolated aperture photometry and optimal photometry (*6*, *7*) on each frame.

The detection of eclipses (*8*) from the hot Jupiter planetary systems HD 209458b (*1*), TrES-1 (*2*), and HD 189733b (*9*) demonstrate that a small fraction (~0.1%) of the total infrared light we observe from these systems is actually emitted from the planet rather than the star. Thus, if we can measure the flux of a system at a signal-to-noise ratio (S/N) > 1000, temperature differences between the day and night faces of the planet will appear as an orbital modulation of the total system flux. With a star as bright as υ Andromedae, our 3-s exposures each have S/N ~ 500, so that our SNR expectation is $\sim\sqrt{160} \times 500 \approx 6300$ at each epoch.

The MIPS instrument acquires data by placing the stellar image in a sequence of 14 positions on the detector. The detector's response varies with position at about the 1% level. This variation is stable and reproducible, so we calculated correction factors as follows: At each epoch, we computed the mean measured system flux at each position and took the ratio with the mean in the first position. We then averaged this ratio over all epochs for each position. This results in corrections < 2% between positions, with uncertainties $\sim 6 \times 10^{-4}$. Bringing the photometry to a common normalization allowed us to average over all the frames in each epoch to achieve S/N ≈ 4350 at each epoch.

As with most infrared instruments, MIPS's sensitivity varies in time. We corrected for such drifts by dividing the system flux value by the measured background in each frame. The background at 24 μm is thermal emission from the zodiacal dust. This dust pervades the inner solar system, absorbing light from the sun and reradiating it at infrared wavelengths. At 24 μm, its emission is strong enough for use as a flux standard, a technique used successfully in measuring the eclipse of HD 209458b (*1*). However, the present work requires one additional correction. The zodiacal background is the integrated emission by dust along the line of sight between the telescope and the object. The observed value thus undergoes an annual modulation as that line of sight varies with the telescope's orbit about the sun. The best available model (*10*) predicts a linear drift over the brief interval of our observations. However, we cannot use the Spitzer model directly, because it is calculated for a line of sight from Earth to the object in question. The difference in position between the Earth-trailing telescope and Earth itself is large enough that the slope of the variation may be slightly different. Thus, we fit for the linear drift directly, simultaneously with any model lightcurve fits.

The phase curve for the υ Andromedae system shows a variation (Fig. 1) in absolute photometry, even before any corrections for instrumental or zodiacal drifts are made. After the calibration with respect to the zodiacal background was applied, this variation is revealed to be in phase with the known orbit of the innermost planet of the system, our principal result.

A simple model can be fit to the phase curve (Fig. 2), assuming local, instantaneous thermal reradiation of the absorbed stellar flux. In the simplest model, the phase of the variation is not a free parameter but is rather set by the measured radial velocity curve (*11*), although phase offsets are possible for models in which the energy is absorbed deep within the atmosphere and redistributed about the surface (*12*, *13*). There is weak (2.5σ) evidence for a small phase offset in this data (Fig. 2), but the large offsets predicted from some models are excluded at high significance. Fitting the peak-to-trough amplitude to the observations yields a best-fit value for the planet-star flux ratio of $2.9 \times 10^{-3} \pm 0.7 \times 10^{-3}$. This is very similar to the result at this wavelength for HD 209458b (*1*). However, the latter is a measure of

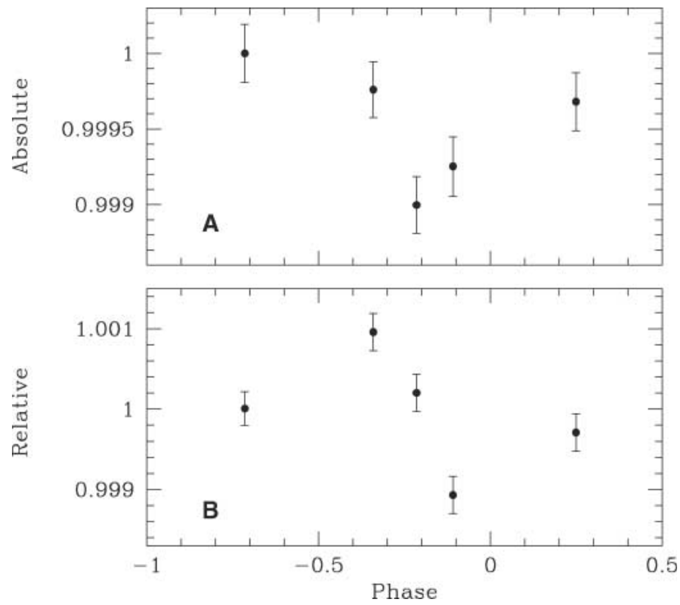

Fig. 1. The light curve of the υ Andromedae system. (**A**) The phase variation in the υ Andromedae system flux before any corrections are applied for instrument or zodiacal drifts. Variations in the system flux are significant even at this point. (**B**) By comparing to the zodiacal background and fitting for the linear drift in the background due to the telescope's motion, we obtained the phase curve shown. In each case, phase is shown modulo unity, with zero phase occurring when the planet is closest to Earth. The amplitude units are expressed in terms of the system flux at the first epoch. Error bars indicate the residual statistical error at each epoch.

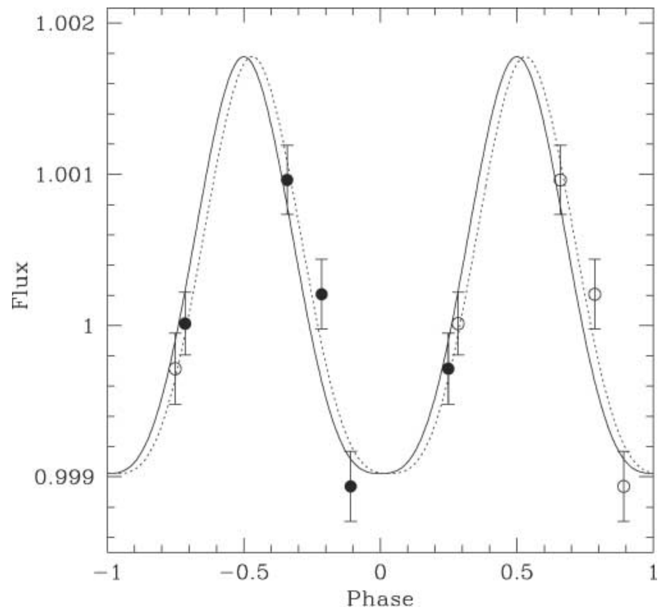

Fig. 2. Comparison of the phase curve and the no-redistribution model. The solid points show our final phase curve, after applying calibrations, in time order from left to right. The open points are repetitions of these, displaced horizontally by one orbit, to better illustrate the phase coverage over two cycles. The solid line is an analytic model for the planetary emission in which energy absorbed from the star is reradiated locally on the day side with no heat transfer across the surface of the planet, the so-called no-redistribution model [and in excellent agreement with the more detailed version in (*17*)]. The assumed inclination in this case is 80° from pole-on, and the relative planet/star amplitude is 2.9×10^{-3}. If we allow for a phase shift relative to the radial velocity curve, we obtain a slightly better fit, as shown by the dotted curve. The best fit is obtained with a phase lag of 11°, but zero lag is excluded only at the 2.5σ level. Error bars indicate the residual statistical error at each epoch.

[1]Department of Physics, University of Central Florida, Orlando, FL 32816, USA. [2]Center for Radiophysics and Space Research, Cornell University, Ithaca, NY 14853, USA. [3]Department of Physics and Astronomy and Institute of Geophysics and Planetary Physics, University of California at Los Angeles, Los Angeles, CA 90095, USA. [4]Department of Astronomy, University of California, Berkeley, CA 94720, USA. [5]Department of Terrestrial Magnetism, Carnegie Institution of Washington, Washington, DC 20015, USA. [6]Planetary Systems Laboratory and Goddard Center for Astrobiology, Goddard Space Flight Center, Greenbelt, MD 20771, USA. [7]Department of Astronomy, Columbia University, New York, NY 10027, USA. [8]Astronomy Unit, School of Mathematical Sciences, Queen Mary, University of London, London E1 4NS, UK. [9]Exoplanets and Stellar Astrophysics Laboratory, Goddard Space Flight Center, Greenbelt, MD 20771, USA.

*To whom correspondence should be addressed. E-mail: hansen@astro.ucla.edu

the absolute flux from the planet divided by that from the host star, whereas the present result is a measure of the flux difference between the projected day and night sides, divided by the flux of the (different) host star.

Another difference between the cases of υ Andromedae b and HD 209458b is that we do not have a strong constraint on the orbital inclination in this system, so we must include the unknown inclination in the model fit (Fig. 3). At higher inclinations, parts of both the night side and the day side are always visible, so the true contrast between the day and night sides must be larger than the amplitude of the observed variation. This contrast is ultimately driven by the light absorbed from the star, which therefore provides an upper limit. We know the distance of the planet from the star and the stellar properties, so we can estimate the contrast that would result if all of the observed flux were reradiated from the day side and nothing from the night side. If we assume the planet's radius is <1.4 Jupiter radii (as observed for other planets of this class), then we can constrain the expected amplitude to be $<3.4 \times 10^{-3}$ (2σ) for a simple black-body, no-redistribution model with zero albedo. Thus, a consistent picture of the atmospheric energetics emerges as long as the orbital inclination is $>30°$.

A natural question to ask is whether there are any plausible alternative models for the observed variation. The estimated rotation period of the star is too long to explain our phase curve as the result of a normal starspot (which is darker than other parts of the stellar surface). One could posit a feature on the stellar surface similar to a starspot but induced by a magnetic interaction between the star and the planet, and therefore moving synchronously with the planet. However, Henry *et al.* (*14*) place an upper limit of 1.6×10^{-4} on the amplitude of optical variation with the planetary orbital period, so infrared variability from the star should be even weaker than this. Some evidence for such magnetospheric interactions is found in observations of chromospheric calcium H and K lines (*15*) and has even been seen in the υ Andromedae system. However, the energy input needed to explain the Ca lines is $\sim 10^{27}$ ergs s^{-1}, much less than the minimum planetary luminosity we infer here ($\sim 4 \times 10^{29}$ ergs s^{-1}). Indeed, one can make a quite general argument that our observations cannot be powered by the same mechanism, because any heating of the star due to magnetic interaction with the planet ultimately extracts energy from the planetary orbit. Thus, one may calculate an orbital decay time

$$\tau = \frac{GM_* M_p}{2a\dot{E}} = 5 \times 10^6 \text{ year} \left(\frac{M_p}{M_J}\right)\left(\frac{a}{12R_\odot}\right)^{-1} \times \left(\frac{\dot{E}}{10^{30} \text{ergs s}^{-1}}\right)^{-1}$$

where M_* and M_p are the stellar and planetary masses, M_J is the mass of Jupiter, a is the semi-major axis, $R_\odot$ is the radius of the Sun, and $\dot{E}$ is the observed heating rate. Heating at the level necessary to explain our observations would result in the decay of the planetary orbit on time scales $< 10^7$ years, yet the estimated age of the system is 3 Giga year. As such, the chromospheric heating of the star is unlikely to be related to the effect seen at 24 μm.

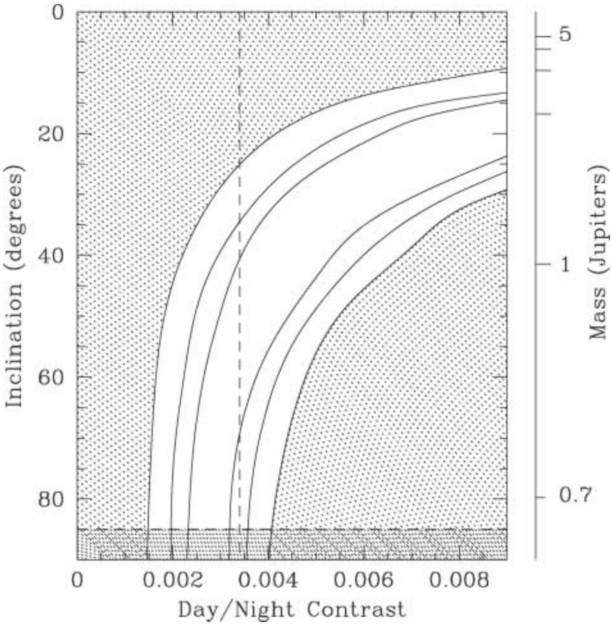

Fig. 3. The influence of inclination on the inferred day-night contrast. The solid contours bound the 1, 2, and 3σ confidence regions for the day-night flux difference (in units of the stellar flux), determined as a function of assumed orbital inclination (measured relative to a face-on orbit). The large shaded regions indicate those values excluded at 3σ. The lower shaded region is excluded because the planet does not transit in front of the star. The vertical dashed line indicates the expected upper limit to the contrast, obtained when the night side is completely dark and all of the stellar flux is reradiated from the day side, in accordance with the no-redistribution model and assuming zero albedo. At the right, we show the true mass of the planet given the assumed inclination (based on the minimum mass derived from the radial velocity curve), in units of Jupiter masses.

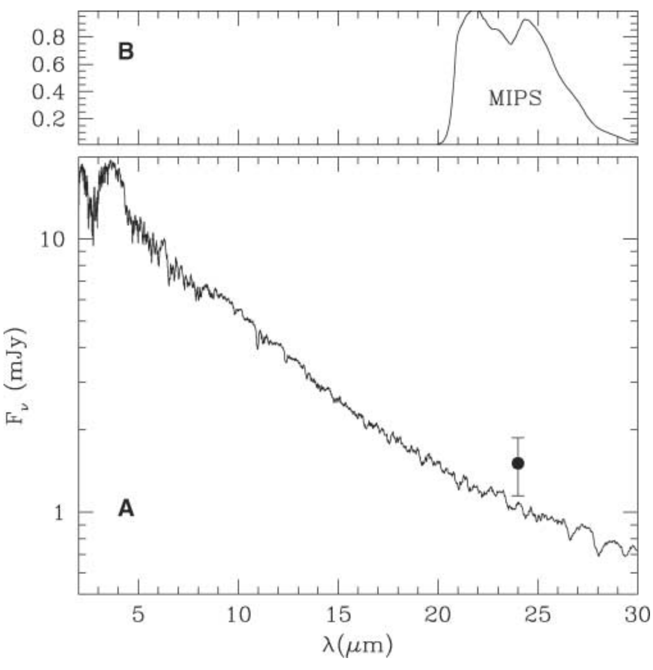

Fig. 4. Comparison of the measured amplitude and a planetary spectral model. (**A**) The solid curve shown is a model (*16*) for a planet of radius $1.4R_J$, irradiated with parameters appropriate to the υ Andromedae system observed at full phase. This results in a temperature ~ 1875 K (*22*). The model is in agreement with the observations (solid circle) at the 2σ level (error bar is 1σ). (**B**) The normalized spectral response curve of the MIPS 24-μm instrument extends from 20 μm to 30 μm.

This observation reveals the presence of a temperature asymmetry on the surface of an extrasolar planet. The first measurements of eclipses (*1*, *2*) yielded measurements of the absolute flux levels emerging from the day sides of two extrasolar planets. When compared with models of radiative transfer in such atmospheres (*16*–*20*), those observations are consistent with a situation intermediate between no redistribution and full redistribution. A similar comparison is possible in this case (Fig. 4). Our observed day-night flux difference is comparable to the flux emerging at full phase in the models of (*16*), which suggests that there is little redistribution of energy to the night side.

In conclusion, the observation of the phase curve of υ Andromedae b indicates that substantial temperature differences exist between the day and night faces of the planet, consistent with a model in which very little horizontal energy transport occurs in the planetary atmosphere. Furthermore, it indicates that the opportunities for direct extrasolar planetary observations are better than previously thought, because useful data can be obtained even in cases where the planetary orbit is not so fortuitously aligned that the system exhibits transits or eclipses.

References and Notes

1. D. Deming, S. Seager, L. J. Richardson, J. Harrington, *Nature* **434**, 740 (2005).
2. D. Charbonneau *et al.*, *Astrophys. J.* **626**, 523 (2005).
3. There is no official terminology for planets that orbit close to their parent stars. The term "hot Jupiter" is the most common, although some authors have adopted other terms, such as "Pegasids," "Pegasi planets," or "Roasters."
4. G. H. Rieke *et al.*, *Proc. SPIE* **5487**, 50 (2004).
5. M. W. Werner *et al.*, *Astrophys. J. Suppl. Ser.* **154**, 1 (2004).
6. K. Horne, *Publ. Astron. Soc. Pac.* **98**, 609 (1986).
7. L. J. Richardson, J. Harrington, S. Seager, D. Deming, *Astrophys. J.*; preprint available at http://arxiv.org/abs/astro-ph/0606096.
8. The passage of an extrasolar planet behind its star, an eclipse, results in a drop in the total system flux. This allows a measurement of the absolute flux emerging from the part of the planet that faces the star (the day side). This is possible when the orbit is aligned almost edge-on to the line of sight.
9. D. Deming, J. Harrington, S. Seager, L. J. Richardson, *Astrophys. J.* **644**, 560 (2006).
10. We use the estimator provided by the Spitzer Science Center, which is based on the DIRBE model described by (*21*). Further information on the specific implementation is given at http://ssc.Spitzer.caltech.edu/documents/background.
11. R. P. Butler *et al.*, *Astrophys. J.* **474**, L115 (1997).
12. J. Cho, K. Menou, B. Hansen, S. Seager, *Astrophys. J.* **587**, L117 (2003).
13. C. S. Cooper, A. P. Showman, *Astrophys. J.* **629**, L45 (2005).
14. G. W. Henry, S. L. Baliunas, R. A. Donahue, C. F. Fekel, W. Soon, *Astrophys. J.* **531**, 415 (2000).
15. E. Shkolnik, G. A. H. Walker, D. A. Bohlender, P.-G. Gu, M. Kürster, *Astrophys. J.* **622**, 1075 (2005).
16. S. Seager *et al.*, *Astrophys. J.* **632**, 1122 (2005).
17. T. Barman, P. Hauschildt, F. Allard, *Astrophys. J.* **632**, 1132 (2005).
18. J. Fortney, M. Marley, K. Lodders, D. Saumon, R. Freedman, *Astrophys. J.* **627**, L69 (2005).
19. A. Burrows, I. Hubeny, D. Sudarsky, *Astrophys. J.* **625**, L135 (2005).
20. D. A. Fischer, J. Valenti, *Astrophys. J.* **622**, 1102 (2005).
21. T. Kelsall *et al.*, *Astrophys. J.* **508**, 44 (1998).
22. The usual estimate given for planetary temperatures is the equilibrium temperature, T_{eq}, defined as the effective temperature of a uniformly bright planet radiating energy at a rate that balances the irradiation received from the star. T_{eq} is thus determined by the stellar effective temperature, T_{eff}, stellar radius, R_*, and distance of the planet from the star a:

$$T_{eq} = 1744\ \mathrm{K}(T_{eff}/6212\ \mathrm{K})(R_*/1.57R_\odot)^{1/2} \times (a/0.059\mathrm{AU})^{-1/2}$$

in the case of υ and b with albedo = 0.05. However, in a proper no-redistribution model, the temperature distribution is not uniform but rather hottest at the substellar point and coolest at the limb, and the full-phase temperature average over the planetary surface is better approximated by $(4/3)^{1/4}T_{eq}$. This is the temperature we adopt, which is 1875 K in this case.

23. This work is based on observations made with the Spitzer Space Telescope, which is operated by the Jet Propulsion Laboratory, California Institute of Technology, under contract with NASA. Support for this work was provided directly by NASA, its Origins of Solar Systems and Astrophysical Theory programs, as well as the Astrobiology Institute and Spitzer Science Center. We thank the personnel of the Spitzer Science Center and its MIPS instrument, who ultimately made these measurements possible.

15 August 2006; accepted 18 September 2006
Published online 12 October 2006;
10.1126/science.1133904
Include this information when citing this paper.

Brownian Motion of an Ellipsoid

Y. Han,[1] A. M. Alsayed,[1] M. Nobili,[2] J. Zhang,[1] T. C. Lubensky,[1]* A. G. Yodh[1]

We studied the Brownian motion of isolated ellipsoidal particles in water confined to two dimensions and elucidated the effects of coupling between rotational and translational motion. By using digital video microscopy, we quantified the crossover from short-time anisotropic to long-time isotropic diffusion and directly measured probability distributions functions for displacements. We confirmed and interpreted our measurements by using Langevin theory and numerical simulations. Our theory and observations provide insights into fundamental diffusive processes, which are potentially useful for understanding transport in membranes and for understanding the motions of anisotropic macromolecules.

Brownian motion (*1*), wherein small particles suspended in a fluid undergo continuous random displacements, has fascinated scientists since before it was first investigated by the botanist Robert Brown in the early 19th century. The origin of this mysterious motion was largely unexplained until Einstein's famous 1905 paper (*2*) that established a relation between the diffusion coefficient of a Brownian particle and its friction coefficient. One year later (*3*), Einstein extended the concept of Brownian dynamics to rotational and other degrees of freedom. The subsequent study of Brownian motion and its generalizations has had a profound impact on physics, mathematics, chemistry, and biology (*4*). Because direct detection of translational Brownian motion is relatively easy, many experiments elucidating the ideas of translational diffusion have been carried out. On the other hand, the direct visualization of rotational Brownian motion has not been an easy task, and fundamental concepts about motions of anisotropic macromolecules remain untested. For this contribution, we used digital video microscopy to study the Brownian motion of an isolated ellipsoid in suspension and thus directly observed the coupling effects between rotational and translational motion.

Particle anisotropy leads to dissipative coupling of translational to rotational motion and to physics first explored by F. Perrin (*5*, *6*). A uniaxial anisotropic particle is characterized by two translational hydrodynamic friction coefficients, γ_a and γ_b, respectively, for motion parallel and perpendicular to its long axis. If a particle's rotation is prohibited, it will diffuse independently in directions parallel and perpendicular to its long axis with respective diffusion constants of $D_\alpha = k_B T/\gamma_\alpha$ for α either a or b, where k_B is Boltzmann's constant and T is the temperature. In general, γ_a is less than γ_b (*7*), and consequently D_a is greater than D_b. If rotation is allowed, rotational diffusion, characterized in two dimensions by a single diffusion coefficient, D_θ, and associated diffusion time, $\tau_\theta = 1/(2D_\theta)$, washes out directional memory and leads to a crossover from anisotropic diffusion at short times to isotropic diffusion at times much longer than τ_θ. Figure 1, A and B, presents numerical simulations (*8*) that illustrate this behavior. Our experiments, which were restricted to two dimensions (2D), provide explicit verification of this behavior and some of its extensions. In addition, we show that a fundamental property of systems with dissipatively coupled translation and rotation is the existence of non-Gaussian probability density functions (PDFs) for displacements in the lab frame.

Micrometer-sized PMMA (polymethyl methacrylate) uniaxial ellipsoids (*9*) were under strong quasi–two-dimensional confinement in a thin glass cell. The choice of 2D rather than 3D for these studies substantially simplified the experimental imaging tasks as well as the data acquisition time and storage requirements. The choice also ensured that the measured effects would be large by virtue of the much larger friction anisotropy in 2D compared with 3D. The local cell thickness was ~1 μm. It was measured to within 0.1 μm resolution by comparing the Michel-Levy chart (*10*) to the reflected interference colors produced by the two inner surfaces under white light illumination on the microscope (Fig. 1D). To avoid interactions between ellipsoids, we made the solution very dilute. The Brownian motion of a single ellipsoid in water was recorded by a charge-coupled device (CCD) camera on a videotape at 30 frame/s. From the image analyses, we obtained data sets consisting of a particle's center-of-mass positions

[1]Department of Physics and Astronomy, University of Pennsylvania, 209 South 33rd Street, Philadelphia, PA 19104, USA. [2]Laboratoire des Colloides, Verres et Nanomateriaux CNRS-University Montpellier II, Place E. Bataillon, 34090 Montpellier, France.

*To whom correspondence should be addressed. E-mail: tom@physics.upenn.edu